Unbalanced Three-Phase LLC Resonant Converters: Analysis and Trigonometric Current Balancing

Sayed Abbas Arshadi, *Student Member, IEEE*, Martin Ordonez, *Member, IEEE*, Wilson Eberle, *Member, IEEE*, Mohammad Ali Saket, *Student Member, IEEE*, Marian Craciun, *Member, IEEE*, and Chris Botting, *Member, IEEE*

***Abstract*—Three-phase LLC resonant converters can handle very high power levels beyond the capabilities of half-bridge and full-bridge LLC topologies. Among other characteristics, three-phase LLC structures reduce output current ripple (small output filter), enable parallel power processing (low peak current), and provide good thermal distribution. However, all these key advantages can be severely compromised due to passive components tolerances, leading to undesired current balance issues in three-phase LLC resonant converters. Tolerances in resonant tank passive components are inevitable and lead to unequal peak currents between phases, uneven temperature distribution, and large output current ripple. This paper investigates the imbalances in three-phase LLC converters and proposes a novel trigonometric current balancing (TCB) technique using phasor analysis. In this strategy, the required input voltage phase angles are calculated to achieve balanced phase currents, even under severe unbalanced conditions. In some cases, the output filter current ripple is reduced to less than half. The methodology is verified with a 3-kW experimental prototype, which validates the analytical framework and effectiveness of TCB.**

***Index Terms*—Current sharing, interleaved resonant converter, three-phase LLC, trigonometric current balancing (TCB).**

I. Introduction

DURING the past decade, LLC resonant converters have gained popularity in many applications especially where there are strict requirements on efficiency, power density, and electromagnetic compatibility (EMC). The popularity is due to the unique features of the LLC resonant converter, which include zero voltage switching for the primary switches and zero current switching for the secondary side rectifier diodes. Soft switching allows higher frequency operation, which reduces the size of passive components and increases the power density [1]–[8].

Manuscript received February 26, 2018; revised May 2, 2018; accepted May 28, 2018. Date of publication June 10, 2018; date of current version February 5, 2019. This work was supported by the Natural Sciences and Engineering Research Council, Canada. Recommended by Associate Editor X. Ruan. *(Corresponding author: Martin Ordonez.)*

S. A. Arshadi, M. Ordonez, W. Eberle, and M. A. Saket are with the Department of Electrical and Computer Engineering, The University of British Columbia, Vancouver, BC V6T 1Z4, Canada (e-mail:

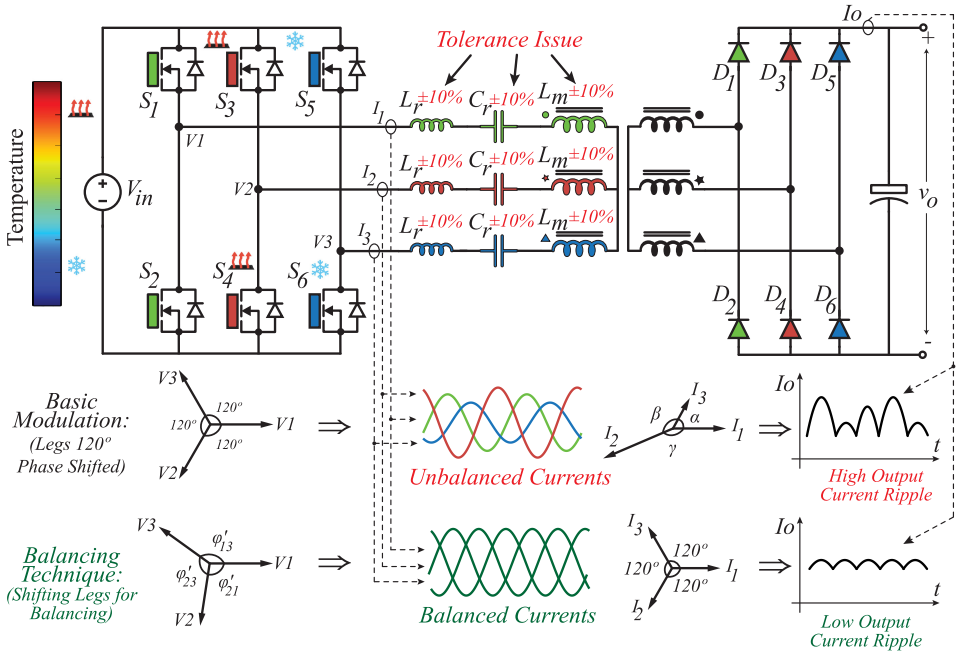

Fig. 1. Resonant components tolerance issue: unbalanced circuit results in unbalanced current, not equally distributed loss and heat in the circuit, and high output current ripple. The proposed balancing technique achieves fully balanced current in an unbalanced circuit and resolves the aforementioned issues.

been presented in [28] and [29]. In those works, PFC rectifiers (3 units) have been employed to regulate the dc input voltages of each LLC phase. While balancing can be achieved, using three separate PFCs or three preregulators can be cost-prohibitive for some applications.

The root cause of unbalanced operation is the tolerance in C_r, L_r, and L_m values of the LLC converter. Normally, 10% change in the passive component values can be expected, leading to detrimental unbalanced currents [30]–[32]. As shown in Fig. 1, unbalanced currents result in unwanted higher output current ripple, unequally distributed loss and consequently temperature in the circuit, higher voltage and current pick values, and higher conduction losses. Due to this unbalanced characteristics, there is a challenge in using three-phase LLC resonant converter effectively. While interesting work, the limited body of the literature on three-phase LLC converters demands more analytical tools to model/explain their behavior and solve fundamental problems, such as current balancing.

In this paper, a detailed analysis of the current-sharing characteristics of the three-phase LLC resonant converter is developed to predict unbalanced operation. The theory shows how the tolerance in components affect the behavior of the converter leading to current balancing issues. In addition, a trigonometric current balancing (TCB) technique is proposed to mitigate the unbalanced behavior of the circuit. In this strategy, the required input voltage phase angles are calculated to achieve balanced phase currents. The switching-angles of the inverter legs are updated (shifted) based on the calculated values. The analysis tool presented in this paper can predict the behavior of the converter, prevent worse-case scenarios, and determine the severity of unbalanced behavior. Fig. 1 conceptually shows the current-sharing issue in the three-phase LLC resonant converter and the proposed TCB technique. TCB successfully balances the three-phase currents, resulting in significant reduction in the output capacitor current ripple and better thermal distribution. Without requiring any additional circuit, this technique provides the opportunity to integrate the advantages of three-phase structures (e.g., high-power and low output current ripple) with the unique features of LLC resonant converter (e.g., high efficiency). In Section II, the current-sharing analysis is presented, and Section III proposes and discusses the TCB. In Section IV, simulation and experimental results of a 3-kW three-phase LLC resonant converter are provided to show the validity of the analysis.

II. Current-Sharing Analysis

As mentioned in Section I, previous works have analyzed three-phase resonant converters with the assumption of the balanced circuit. Assuming the balanced condition, these papers have derived a single-phase equivalent circuit for the converter that can be used to analyze the characteristics of the converter. However, this type of analysis cannot be used to investigate the unbalanced behavior of the LLC resonant converter. In this section, a three-phase equivalent circuit of the LLC resonant converter is developed, which can be used to analyze the characteristics of the converter and provides the detailed insight into the effect of Ls, Cs, and L_m values. Therefore, the resulting analysis can be used to evaluate current sharing even under unbalanced conditions.

The three-phase LLC resonant converter, as shown in Fig. 1, is formed by a three-phase dc–ac inverter, three resonant tanks, a high-frequency three-phase transformer or three single-phase transformers connected in star with floating star point, and a three-phase full-bridge rectifier. Similar to the half-bridge and full-bridge resonant converters, the three-phase converter applies square wave voltages to the input of the resonant network.

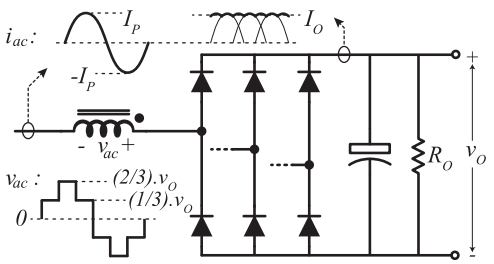

Fig. 2. Effective load reflected on each of the secondaries windings of the transformers considering FHA.

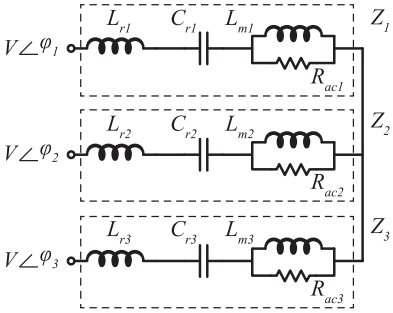

Fig. 3. Equivalent three-phase circuit of the converter.

The resonant network filters the harmonics of the input voltages in a way that three sinusoidal currents appear. This allows using ac analysis techniques for analyzing the behavior of the converter. Considering the filtering characteristics of the resonant tanks, it is possible to approximate the square input voltage waveforms with the fundamental component and compute the resulting sine waves of current and voltage in the resonant tank with good precision.

To do so, it is necessary to model the capacitive output rectifier. As shown in Fig. 2, the input voltage of each of the diode bridges is a five-level square waveform, which is essentially the voltage across the secondary of the transformers. The fundamental harmonic of this voltage can be calculated using Fourier series as (1), where *T* is the switching period. Assuming pure sinusoidal waveforms, the root-mean-square (RMS) value of the current through the transformer winding as a function of output current can be calculated as follows:

$$V_{ac,rms} = \frac{\sqrt{2}}{\pi}\int_0^T v_{ac}(t)\sin\left(\frac{2\pi t}{T}\right)\,\mathrm{d}t = \frac{\sqrt{2}}{\pi}V_O \tag{1}$$

$$I_O = \frac{6}{2\pi}\int_{\frac{\pi}{3}}^{\frac{2\pi}{3}} \sqrt{2}I_{ac,rms}(t)\sin(\omega t)\,\mathrm{d}t = \frac{3\sqrt{2}}{\pi}I_{ac,rms}$$

$$\Rightarrow I_{ac,rms} = \frac{\pi}{3\sqrt{2}}I_O. \tag{2}$$

Using (1) and (2), the equivalent load reflected to the primary of each transformer can be calculated as (3), where *N* is the turns ratio of the secondary to primary of the transformers. Assuming a balanced circuit, the equivalent three-phase circuit of the converter can be extracted, as shown in Fig. 3

$$R_{ac} = N^2\frac{V_{ac,rms}}{I_{ac,rms}} = \frac{6}{\pi^2}N^2R_O. \tag{3}$$

Considering the KVL and KCL in the circuit in Fig. 3, the set of equations in (4) can be extracted

$$\begin{cases} V_2 - V_1 + Z_1I_1 - Z_2I_2 = 0 & \text{(I)} \\ V_3 - V_1 + Z_1I_1 - Z_3I_3 = 0 & \text{(II)} \\ I_2 + I_3 + I_1 = 0 & \text{(III)} \end{cases} \tag{4}$$

where V_1, V_2, and V_3 are the fundamental components of the square wave voltage at the input of each phase, I_1, I_2, and I_3 are the current through the phases, and Z_1, Z_2, and Z_3 are the impedance of each phase, which can be calculated as follows:

$$Z_t = L_{rt}j\omega + \frac{1}{C_{rt}j\omega} + \frac{L_{mt}R_{act}j\omega}{R_{act} + L_{mt}j\omega}, \quad t = 1,2,3 \tag{5}$$

$$Z_t = \left(L_{rt}\omega - \frac{1}{C_{rt}\omega} + \frac{L_{mt}R_{act}^2\omega}{R_{act}^2 + L_{mt}^2\omega^2}\right)j + \frac{L_{mt}^2R_{act}\omega^2}{R_{act}^2 + L_{mt}^2\omega^2}, \quad t = 1,2,3. \tag{6}$$

Using the equations in (4), three-phase currents as a function of input voltages can be calculated as follows:

$$\begin{bmatrix} I_1 \\ I_2 \\ I_3 \end{bmatrix} = \left(\frac{1}{Z_1Z_2 + Z_2Z_3 + Z_1Z_3}\right) \times \begin{bmatrix} Z_2+Z_3 & -Z_3 & -Z_2 \\ -Z_3 & Z_1+Z_3 & -Z_1 \\ -Z_2 & -Z_1 & Z_1+Z_2 \end{bmatrix}\begin{bmatrix} V_1 \\ V_2 \\ V_3 \end{bmatrix}. \tag{7}$$

The above-mentioned equations and the three-phase equivalent circuit in Fig. 3 can be used to find currents in different phases under unbalanced conditions. In the following, the circuit under balanced and unbalanced conditions is analyzed.

A. Balanced Circuit

In a balanced circuit, where $L_{r1} = L_{r2} = L_{r3} = L_r$, $C_{r1} = C_{r2} = C_{r3} = C_r$, $L_{m1} = L_{m2} = L_{m3} = L_m$, and consequently $Z_1 = Z_2 = Z_3 = Z$, (7) can be expressed as follows:

$$\begin{bmatrix} I_1 \\ I_2 \\ I_3 \end{bmatrix} = \left(\frac{1}{3Z}\right)\begin{bmatrix} 2 & -1 & -1 \\ -1 & 2 & -1 \\ -1 & -1 & 2 \end{bmatrix}\begin{bmatrix} V_1 \\ V_2 \\ V_3 \end{bmatrix}. \tag{8}$$

Since the amplitude of the input voltages are equal, and they are 120° phase shifted, the relation between input voltages can be expressed as (9). Using (8) and (9), the three phase currents in a balanced circuit can be calculated as (10)

$$V_1 + V_2 + V_3 = 0 \tag{9}$$

$$I_t = \frac{V_t}{Z}. \tag{10}$$

Equation (10) shows that the currents through the phases are equal and they can be calculated independently from the impedance values of the other phases. This also shows the validity of the single-phase equivalent model for the balanced three-phase LLC resonant converter.

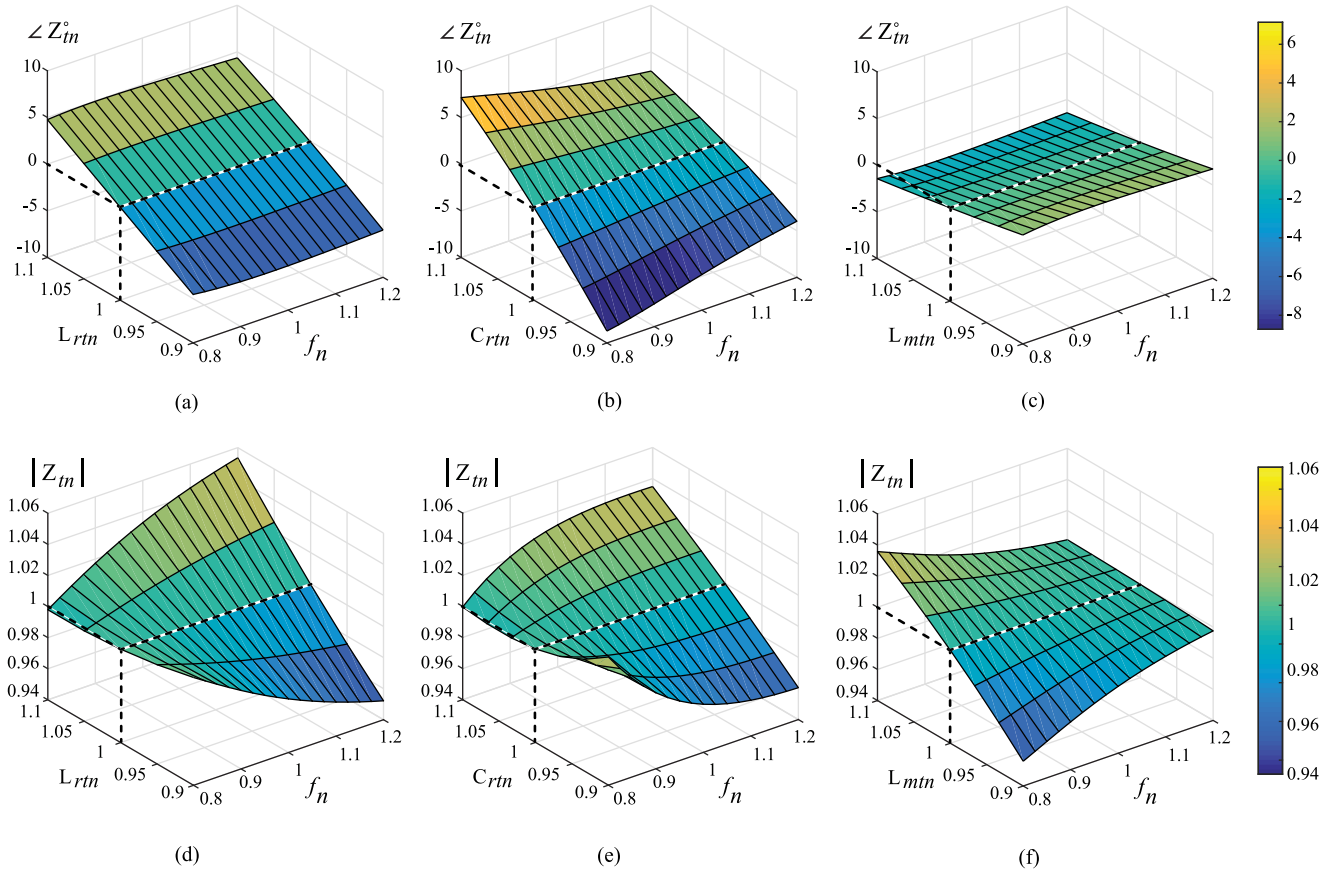

Fig. 4. Effect of 10% tolerance in the values of each of the resonant components of each phase on the amplitude and phase angle of the phase. Changes in the values of L_{rtn} and C_{rtn} show the same trend of changes in the impedance values. The impedance values are less sensitive to the changes in the value of L_{mtn}.

B. Unbalanced Circuit

In the case of an unbalanced circuit, the single-phase equivalent circuit cannot help with the understanding of unbalanced currents. In this case, the three-phase equivalent circuit shown in Fig. 3 and (6) and (7) can be used for analyzing the behavior of unbalanced currents through the phases. This analysis is based on two approximations: first, first harmonic approximation (FHA), and second, approximating unbalanced reflected loads to the primary with equal values of R_{ac}. It will be shown that the impedance value of each phase is less sensitive to the variations in the values of L_{mtn} and R_{ac} in comparison with L_{rtn} and C_{rtn}. Moreover, L_{mtn} and R_{ac} voltages are clamped to the output voltage during most of the operating modes and do not participate in resonance in most of the operating modes. Therefore, while these approximations make the analysis simpler, they achieve results that are accurate enough to show the trend in the changes of three-phase currents in correspondence to specified tolerances in resonant tank elements. The ultimate purpose of the analysis is to find out about the worst-case scenario in current sharing.

1) Worst-Case Investigation: Analyzing the circuit shown in Fig. 3, with nine unknown variables, is difficult to start with. In order to reduce the number of unknown variables, the analysis can be started by investigating the tolerance effect of the resonant tank components of each phase on the impedance value of the corresponding phase. Fig. 4 shows the effect of variations in the value of each resonant element on the impedance of the resonant tank. This figure is based on the design parameters of Section IV and is derived using (6). These plots show the normalized values of the phase angle and amplitude of the impedance versus normalized values of frequency and normalized values of the resonant components. The impedance values and resonant component values are normalized based on the balanced value, and the frequency is normalized based on the resonant frequency (f_r) value as the following:

$$|Z_{tn}| = \frac{|Z_t|}{|Z_{to}|}, \quad \angle Z_{tn} = \angle Z_t - \angle Z_{to}, \quad L_{rtn} = \frac{L_{rt}}{L_{rto}}$$
$$C_{rtn} = \frac{C_{rt}}{C_{rto}}, \quad L_{mtn} = \frac{L_{mt}}{L_{mto}}, \quad f_n = \frac{f}{f_r}. \tag{11}$$

Fig. 4(a) shows that by changing the value of L_{rt} by 10%, the phase angle of $Z_t n$ will be changed up to 5° in the same direction. Fig. 4(b) also shows that changes in the values of C_{rt} have the same effect. Moreover, Fig. 4(d) and (e) shows that changes in the values of L_{rt} or C_{rt} will correspond to the same trend in changes of the impedance amplitude. However, Fig. 4(c) shows that changes in L_{mt} have an opposite effect on phase angle of the impedance compared to the changes in L_{rt} and C_{rt}. Changing the value of L_{mt} by 10% will result in changing the phase angle of the impedance by less than 2°. This

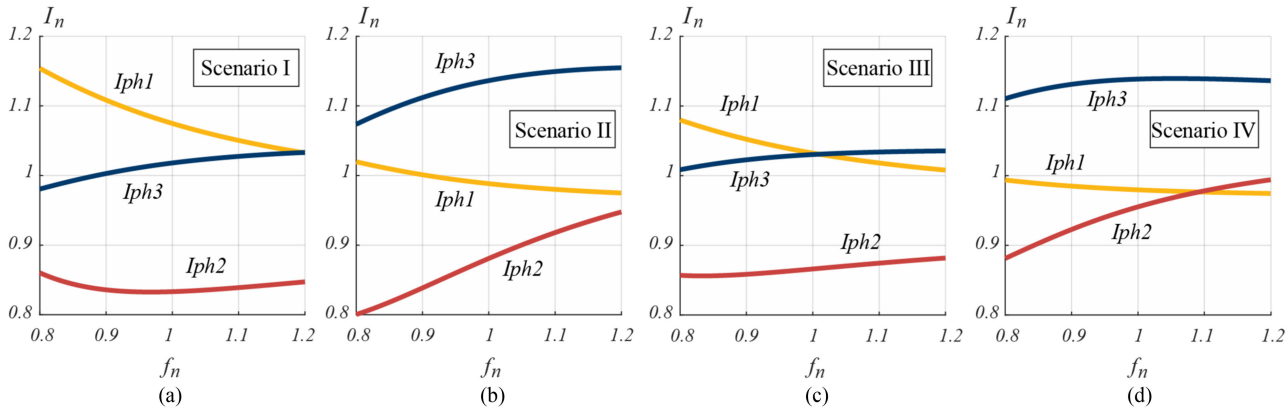

Fig. 5. Trend in changes in the current values in correspondence with four possible worst case scenarios. For (a) and (c), one of the phases carries much less current compared to the other two phases. For (b) and (d), one of the phases carries much higher current compared to the other two phases.

shows that the phase angle of Z_tn is less sensitive to changes of L_{mt}. Moreover, changes in L_{mt} have the same effect on the impedance amplitude as L_{rt} and C_{rt}. However, the trend is not the same over the changes of frequency [see Fig. 4(f)]. This information can be summarized as follows.

1) Changes in L_{rt} and C_{rt} have the same effect on phase angle and amplitude of the impedance. Hence, considering the definition of resonant frequency, expressed in (12), it can be said that changes in the resonant frequency will affect the phase angle and the amplitude of the impedance of each phase. It means that, by changing L_{rt} and C_{rt} in the same direction, which essentially means changing the resonant frequency, the most amount of deviation in the value of impedance will be caused

$$f_r = \frac{1}{2\pi\sqrt{L_{rt}C_{rt}}}. \tag{12}$$

2) Changes in L_{mt} have an opposite effect on the impedance phase angle compared to the effect of L_{rt} and C_{rt}. It means that, by changing the value of L_{mt} and simultaneously changing the value of L_{rt} in the opposite direction, the most deviation in the value of the impedance phase angle will result. Considering the inductor ratio (m), which is expressed as (13), it can be said that changes in the value of m will affect the impedance phase angle. In other words, changing L_{mt} and L_{rt} in opposite directions, which essentially means changing the inductor ratio (m), will result in the most amount of deviation in the value of impedance phase. The changes in L_{mt} have an opposite effect on the impedance amplitude in comparison with its effect of changes on the impedance phase angle. Also, the changes in L_{mt} have an opposite effect on the impedance amplitude over the frequency range in comparison with L_{rt} and C_{rt}. Therefore, it can be said that changes in the value of m can have different impacts on the impedance values and current sharing in the system over the frequency range

$$m_t = \frac{L_{mt}}{L_{rt}}. \tag{13}$$

TABLE I
POSSIBLE WORST-CASE SCENARIOS OF UNBALANCED IMPEDANCES

	Levels		
	Phase 1	Phase 2	Phase 3
Scenarios	f_r, L_m	f_r, L_m	f_r, L_m
Case I	min, min	min, min	max, max
Case II	min, min	max, max	max, max
Case III	min, max	min, max	max, min
Case IV	min, max	max, min	max, min

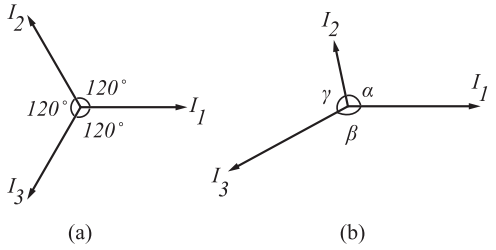

Fig. 6. Law of sines. (a) Balanced currents with ideal components. (b) Unbalanced currents with real components with tolerances.

3) The impedance phase angle and amplitude are much more sensitive to the changes in the values of L_{rt} and C_{rt} than to the value of L_{mt}.

The worst case in current sharing is when two of the phases have lower current, and the other phase takes the highest current. In this situation, the phase with higher current experiences the highest pick values, highest losses, and highest temperature rise. To find out about the worst case in current sharing, it is necessary to investigate different possible worst-case unbalanced scenarios. Based on the information above, the worst-case deviation in the value of the impedance of each phase happens when the resonant frequency (f_r) and the inductor ratio (m) of that phase changes. Therefore, based on the possible combination of tolerances in f_r and L_{mt}, four of the possible scenarios can be as

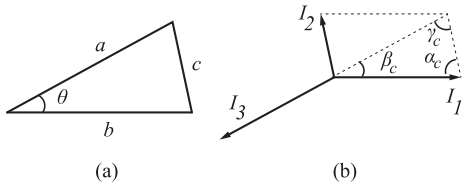

Fig. 7. Law of cosines. (a) Triangular. (b) Triangular in three-phase current vectors.

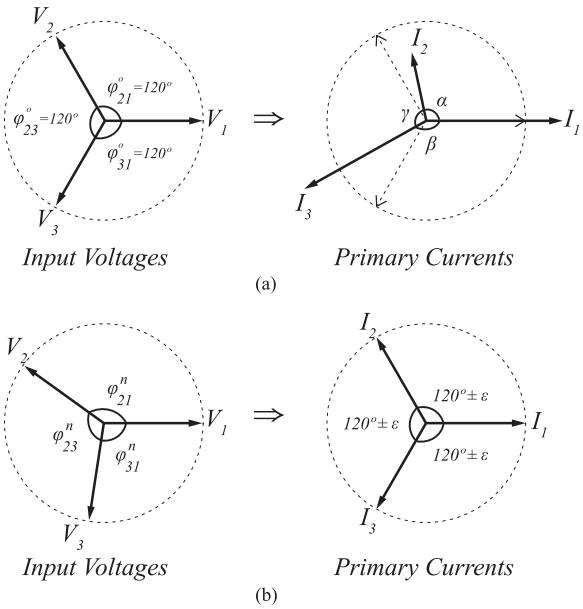

Fig. 8. Balancing technique. (a) Basic 120° phase-shifted input voltages. (b) Balancing currents with changing the phase-shift of the input voltages.

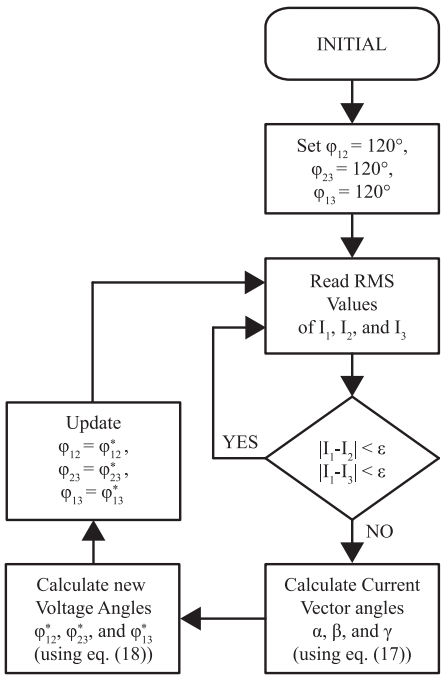

Fig. 9. Trigonometric current balancing technique flowchart.

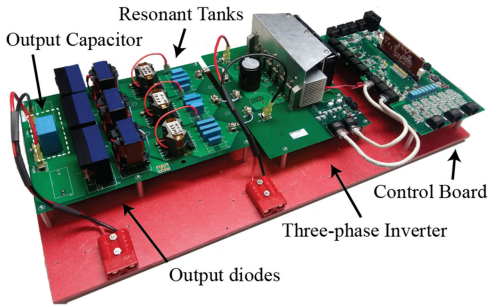

Fig. 10. 3-kW experimental setup. Reduced output filter size due to the output current ripple reduction.

TABLE II
DESIGNED PARAMETERS OF THE EXPERIMENTAL SETUP

Parameter	Values
V_{in}	$400V$
V_{out}	$300-400V$
$P_{out}(max)$	$3kW$
$I_{out}(max)$	$10A$
n_1/n_2	$12/3$
f_r	$205kHz$
m	3
L_r	$20\mu H \pm 10\%$
C_r	$30nF \pm 10\%$
L_m	$60\mu H \pm 10\%$

TABLE III
EXPERIMENTALLY VERIFIED VALUES OF RESONANT COMPONENTS

	Ideal components		
Phases	L_r $[\mu H]$	C_r $[nF]$	L_m $[\mu H]$
Phase I	20	30	60
Phase II	20	30	60
Phase III	20	30	60
	Real components (Experimental setup)		
Phases	L_r $[\mu H]$	C_r $[nF]$	L_m $[\mu H]$
Phase I	23	33.2	59
Phase II	18.7	26.8	58.6
Phase III	18	26.9	57.5

These values are corresponding to the discussed worst-case scenarios.

shown in Table I, where

$$\begin{cases} f_r(\min) = \frac{1}{2\pi\sqrt{(L_r+10\%)(C_r+10\%)}} \\ \qquad\qquad L_m(\min) = L_m - 10\% \\ f_r(\max) = \frac{1}{2\pi\sqrt{(L_r-10\%)(C_r-10\%)}} \\ \qquad\qquad L_m(\max) = L_m + 10\%. \end{cases} \tag{14}$$

In order to investigate the corresponding current sharing of each scenario, Fig. 5 shows three-phase currents as a function of normalized frequency for different scenarios. In this figure,

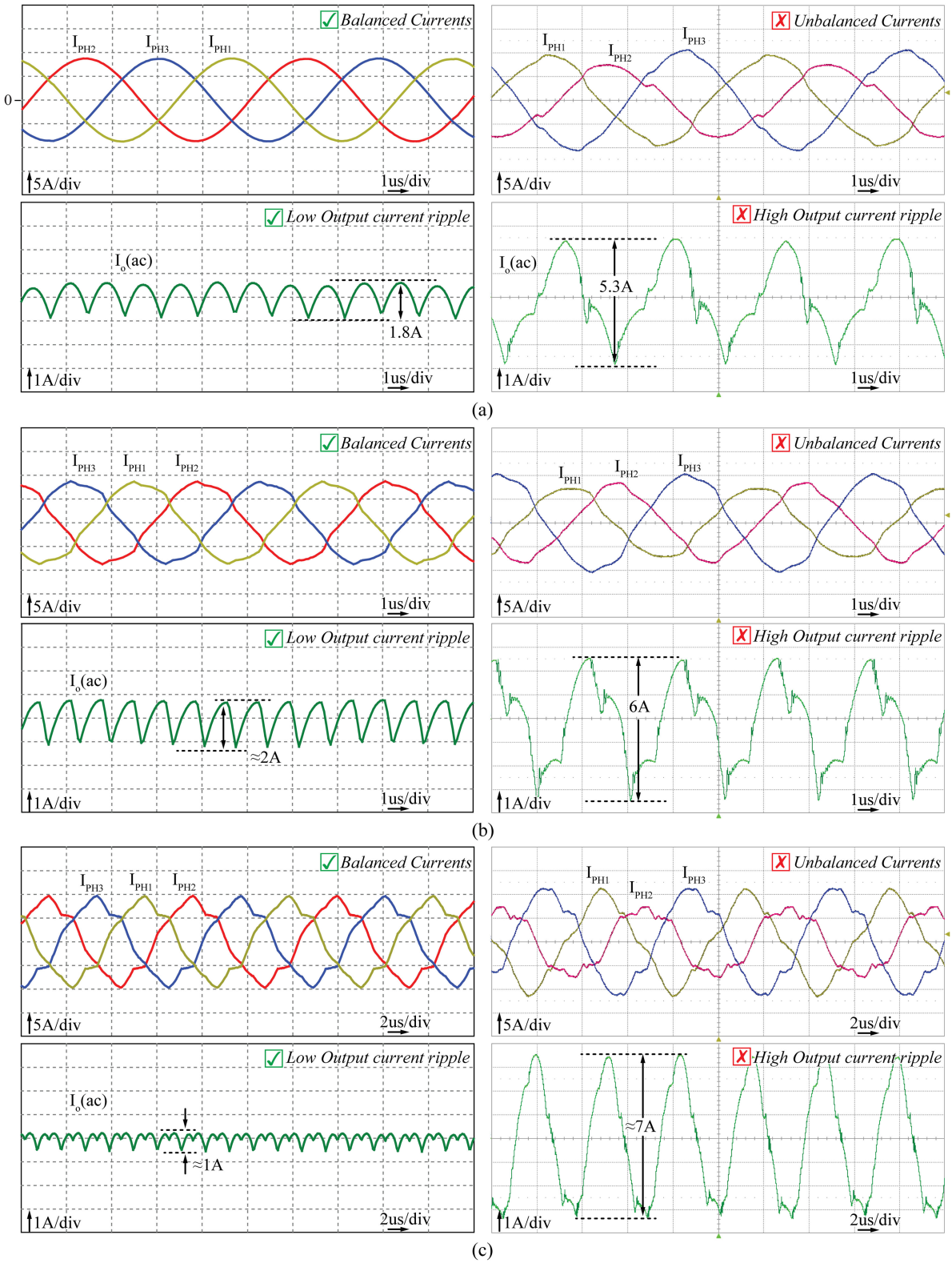

Fig. 11. Simulation results of the ideal circuit (left-hand side) versus the results of the real unbalanced circuit (right-hand side). (a) At resonant frequency. (b) Above resonant frequency. (c) Below resonant frequency. Due to components' tolerances, unbalanced currents are generated in the experimentally implemented circuit. As a result, the output current ripple in the experimental results is significantly higher than the ripple in the ideal circuit. Moreover, the unbalanced behavior results in unequal conduction power loss in the circuit and unequal thermal distribution.

TABLE IV
SIMULATION RESULTS OF THE IDEAL CIRCUIT AND EXPERIMENTAL RESULTS OF THE UNBALANCED CIRCUIT UNDER DIFFERENT CONDITIONS

	Below resonant frequency		
Parameters	Ideal Circuit	Real Circuit	TCB Results
Primary currents (rms) [A]	$I_{ph1}: 6.3$ $I_{ph2}: 6.3$ $I_{ph3}: 6.3$	$I_{ph1}: 6.85$ $I_{ph2}: 5.23$ $I_{ph3}: 7.65$	$I_{ph1}: 6.44$ $I_{ph2}: 6.25$ $I_{ph3}: 6.45$
Output current ripple [A]	1	7	3
Unbalanced factor (U_f)	0%	23.5%	2%
Efficiency [%]	–	96.65	96.9
Input voltage vectors angles	$\phi_{12}: 120^\circ$ $\phi_{13}: 120^\circ$ $\phi_{23}: 120^\circ$	$\phi_{12}: 120^\circ$ $\phi_{13}: 120^\circ$ $\phi_{23}: 120^\circ$	$\phi_{12}: 141^\circ$ $\phi_{13}: 106^\circ$ $\phi_{23}: 113^\circ$
	At resonant frequency		
Parameters	Ideal Circuit	Real Circuit	TCB Results
Primary currents (rms) [A]	$I_{ph1}: 6.3$ $I_{ph2}: 6.3$ $I_{ph3}: 6.3$	$I_{ph1}: 6.8$ $I_{ph2}: 4.7$ $I_{ph3}: 7.3$	$I_{ph1}: 6.25$ $I_{ph2}: 6.36$ $I_{ph3}: 6.22$
Output current ripple [A]	1.8	5.3	2.4
Unbalanced factor (U_f)	0%	25.6%	1.5%
Efficiency [%]	–	96.8	97.2
Input voltage vectors angles	$\phi_{12}: 120^\circ$ $\phi_{13}: 120^\circ$ $\phi_{23}: 120^\circ$	$\phi_{12}: 120^\circ$ $\phi_{13}: 120^\circ$ $\phi_{23}: 120^\circ$	$\phi_{12}: 141^\circ$ $\phi_{13}: 98^\circ$ $\phi_{23}: 121^\circ$
	Above resonant frequency		
Parameters	Ideal Circuit	Real Circuit	TCB Results
Primary currents (rms) [A]	$I_{ph1}: 5.9$ $I_{ph2}: 5.9$ $I_{ph3}: 5.9$	$I_{ph1}: 6.20$ $I_{ph2}: 4.89$ $I_{ph3}: 6.96$	$I_{ph1}: 5.85$ $I_{ph2}: 5.95$ $I_{ph3}: 6.00$
Output current ripple [A]	2	6	3.3
Unbalanced factor (U_f)	0%	22%	1.7%
Efficiency [%]	–	96.46	96.72
Input voltage vectors angles	$\phi_{12}: 120^\circ$ $\phi_{13}: 120^\circ$ $\phi_{23}: 120^\circ$	$\phi_{12}: 120^\circ$ $\phi_{13}: 120^\circ$ $\phi_{23}: 120^\circ$	$\phi_{12}: 154^\circ$ $\phi_{13}: 100^\circ$ $\phi_{23}: 106^\circ$

Comparing the results of the ideal and real circuit, it is clear that the output current ripple is much higher in the real circuit. Moreover, it is clear that the proposed TCB successfully balances the currents and significantly reduces the output current ripple.

normalized RMS values of currents (normalized based on the value of balanced circuit) versus the normalized frequency are depicted. As it can be seen, the cases in scenarios II and IV seem to be worse than the other two scenarios. In these two scenarios, two of the phases have the maximum resonant frequency (f_r) and the other phase has the minimum f_r. On the other hand, the behavior of L_m in affecting the current sharing is quite unpredictable. Comparing Fig. 5(a) and (c), or (b) and (d), it can be concluded that by changing the value of L_m from its minimum to its maximum, the trend of current curves does not change significantly. This confirms the small effect of the tolerances on the values of L_m of different phases on the current-sharing behavior of the circuit.

The analytical results of the three-phase circuit show that in the worst-case scenario, in which two of the phases have maximum resonant frequency and the other phase has the minimum resonant frequency, one of the phases may need to handle currents up to 15% more than its rated current.

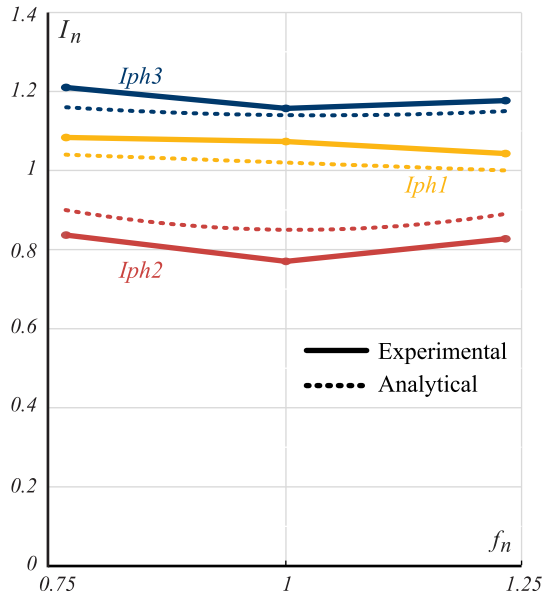

Fig. 12. Current-sharing trend prediction with the proposed analysis versus the experimental results. The analysis reasonably predicts the trend of changes in the currents with the given components' values.

III. TCB Technique

In Section II, it was shown how the tolerance in the values of resonant components can affect the impedance value of each phase and how it would generate unbalanced currents through the phases. As mentioned in Section I, unbalanced currents in the converter result in loss of some of the features of the three-phase structure. Unequally distributed losses in the circuit, developing hotspots, and not having perfect output current ripple cancellation, meaning much higher output current ripple, are some of the disadvantages of having unbalanced currents. In this section, the detailed analytical framework developed is used to develop a TCB technique in an unbalanced circuit.

A. Law of Sines and Law of Cosines

The law of sines shows the relation among the angles and the lengths of sides of a triangle, which can also be used for the current vectors in a three-phase circuit. Considering the FHA and using the law of sines, it can be shown that if the amplitudes of the currents in a three-phase circuit are equal, then they are 120° phase shifted. Accordingly, if the currents are not balanced, it can be concluded that the angles between the current vectors are no longer equal. Moreover, based on the order of the current amplitudes, the order of angles between the vectors can be realized. Fig. 6 shows the current vectors in a balanced circuit and unbalanced circuit, conceptually. Using the law of sines, the relationships between vectors and angles is presented in the following equation:

$$\begin{cases} \text{if} & |I_1| = |I_2| = |I_3| \iff \beta = \gamma = \alpha \\ \text{if} & |I_1| \neq |I_2| \neq |I_3| \iff \beta \neq \gamma \neq \alpha \\ \text{if} & |I_1| > |I_2| > |I_3| \iff \alpha > \beta > \gamma. \end{cases} \tag{15}$$

The exact value of the angles between the current vectors can be calculated using the law of cosines. The law of cosines in conjunction with the law of sines can help in finding all sides and angles of a triangular. In a basic triangular as shown in Fig. 7(a), where the sides are known, the angle between two of the sides can be calculated using the law of cosine as follows:

$$\cos\theta = \frac{a^2 + b^2 - c^2}{2ab}. \tag{16}$$

In three-phase current vectors, a triangular, as shown in Fig. 7(b), can be identified. In this triangular, α_c, β_c, and γ_c are the complementary angles of the angles between the current vectors. Therefore, the angles between current vectors can be calculated as follows:

$$\begin{cases} \alpha = \pi - \arccos\left(\frac{I_1^2 + I_2^2 - I_3^2}{2I_1 I_2}\right) \\ \beta = \pi - \arccos\left(\frac{I_1^2 + I_3^2 - I_2^2}{2I_1 I_3}\right) \\ \gamma = \pi - \arccos\left(\frac{I_2^2 + I_3^2 - I_1^2}{2I_2 I_3}\right). \end{cases} \tag{17}$$

B. TCB Technique

Based on the law of sines, if the angles between the current vectors are corrected to be equal to 120°, the currents will be balanced. Assuming an unbalanced circuit in Fig. 3, there are two variables that can be manipulated by switching the MOSFETs: the amplitudes and the phase angles of the input voltages. The amplitude of the input voltages can be controlled by PWM, and the phase angle can be simply controlled by phase shifting the input voltages. Implementing PWM in LLC resonant converters has some limitations due to the possibility of losing soft switching for the MOSFETs, and of changes in the converter gain. In the following, a TCB technique for three-phase LLC resonant converter based on shifting the phase of the inverter bridge's switching points is presented.

Fig. 8(a) shows the current vectors in an unbalanced circuit with the basic 120° phase-shifted input voltage vectors. The idea to correct the angles between of unbalanced current vectors is to change the angles between the input voltage vectors in a way that it results in shifting the current vector angles toward 120°. For example, in Fig. 8(a), α is less than 120°, and β is larger than 120°. In this case, reducing ϕ_{31} and increasing ϕ_{12} can result in increasing α and decreasing β [see Fig. 8(b)]. Fig. 9 shows the flowchart of the proposed balancing technique. Different steps of the proposed TCB are as follows.

1) Initially, the phase angles between the input voltage vectors are 120° by default. If the circuit is unbalanced, this will result in unbalanced currents in the circuit.
2) The balancing technique is based on balancing the RMS values of the currents. This is because the RMS value is a better representative of the first harmonic of the currents compared to peak or mean rectified values. As mentioned previously, the balancing technique is based on the FHA and balancing the fundamental harmonic of the currents. Moreover, RMS value of the current is directly related to

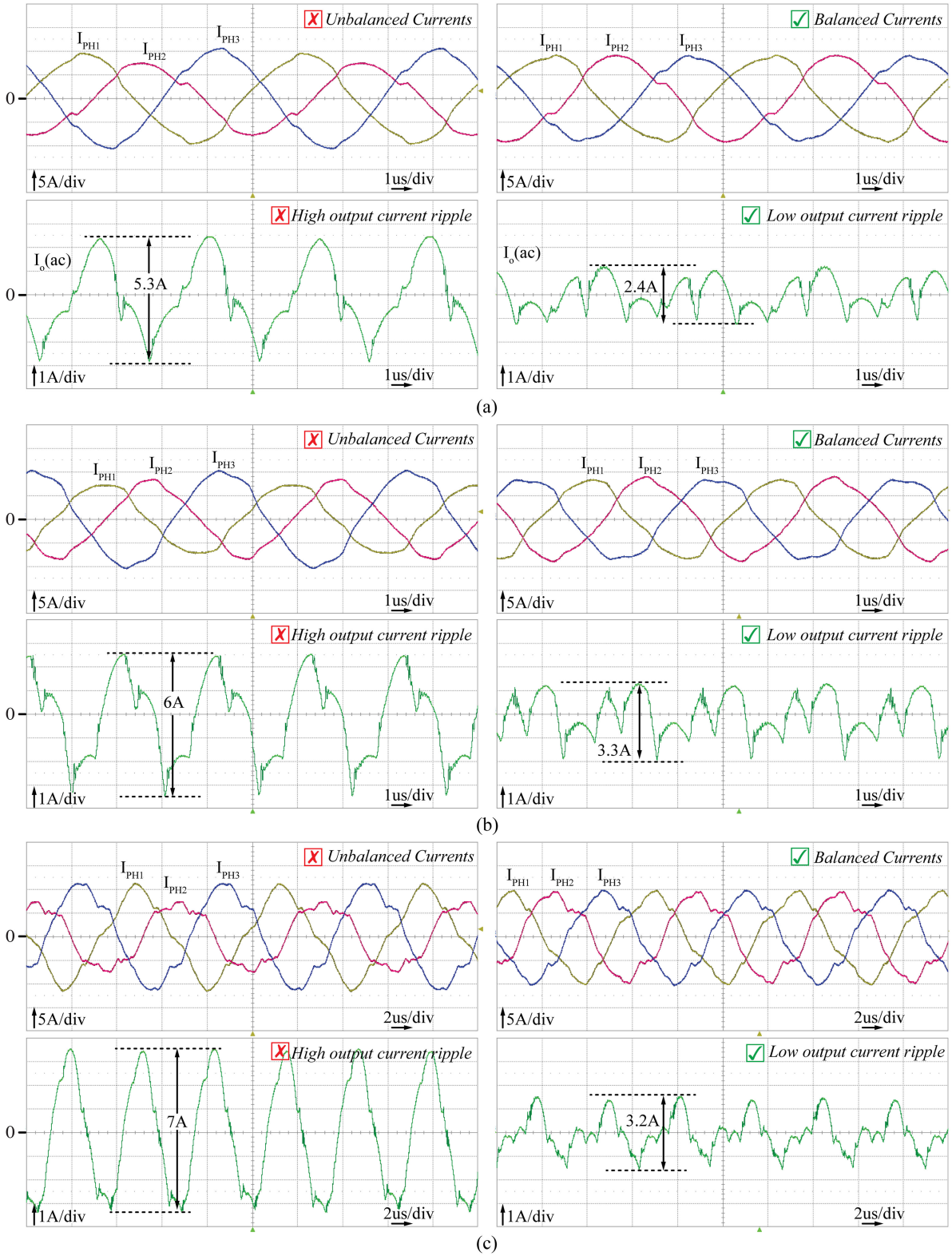

Fig. 13. Results of the unbalanced circuit without TCB (left-hand side) versus the results of TCB (right-hand side). (a) At resonant frequency. (b) Above resonant frequency. (c) Below resonant frequency. Using the proposed TCB, the primary currents are perfectly balanced, and as a result, the output current ripple is significantly reduced.

the conduction losses. Hence, balancing RMS values will result in equal losses through the phases.

3) After reading the current RMS values, they are compared to see if the difference between RMS values is less than the specified threshold. If they were close enough, the process of reading the values and comparing them continuously occurs. If the differences in currents are not within the limit, TCB starts.
4) The angles between the current vectors (α, β, and γ) are calculated using (17).
5) New switching angles based on the current vector angles are defined using the following equation:

$$f(\phi): \begin{cases} \phi_{12}^{\star} = \phi_{12} + (120^{\circ} - \alpha) \\ \phi_{13}^{\star} = \phi_{13} + (120^{\circ} - \beta) \\ \phi_{23}^{\star} = \phi_{23} + (120^{\circ} - \gamma). \end{cases} \tag{18}$$

In this equation, $\phi^{\star}$ is the new voltage vector angle, and ϕ is the angle of the previous stage. At this point, the voltage vectors are phase shifted with the same amount of deviation in the current vector angles from 120°.

6) After the new switching angles are defined, the inverter legs are shifted based on the new switching points, and then the control circuit goes back to step one.

IV. Experimental Results

In order to confirm the validity of the analysis and the proposed TCB technique, extensive experimental tests and simulations have been done. A 3-kW three-phase LLC resonant converter with the proposed control technique has been manufactured and tested under different conditions. Fig. 10 shows the prototype, and the specifications of this platform are presented in Table II. This design can be used for a plug-in hybrid electric vehicle (PHEV) battery charger application. The maximum power and the output current of this converter are 3 kW and 10 A, respectively. Table III shows the experimentally verified values of the resonant components. The values are corresponding to the worst-case scenarios discussed in Section II. The experimental and simulation results are presented in two parts: simulation results of ideal circuit versus the experimental results of the real unbalanced circuit; and results of the TCB applied to the unbalanced circuit versus the results without TCB.

To get a better understanding of unbalanced conditions and to better describe it, an unbalanced factor is defined as (19). This unbalanced factor (U_f) is defined based on the worst potential difference in the conduction losses between the phases. Conduction losses are proportional to the square values of RMS currents, and can represent the potential temperature difference caused by unbalanced currents. Moreover, the output current ripple value is another factor for describing unbalanced currents. As there are more unbalanced currents, the output current ripple will be higher

$$U_f = \frac{\text{Max}(I_{ph1}^2, I_{ph2}^2, I_{ph3}^2) - \text{Min}(I_{ph1}^2, I_{ph2}^2, I_{ph3}^2)}{I_{ph1}^2 + I_{ph2}^2 + I_{ph3}^2} \times 100\%. \tag{19}$$

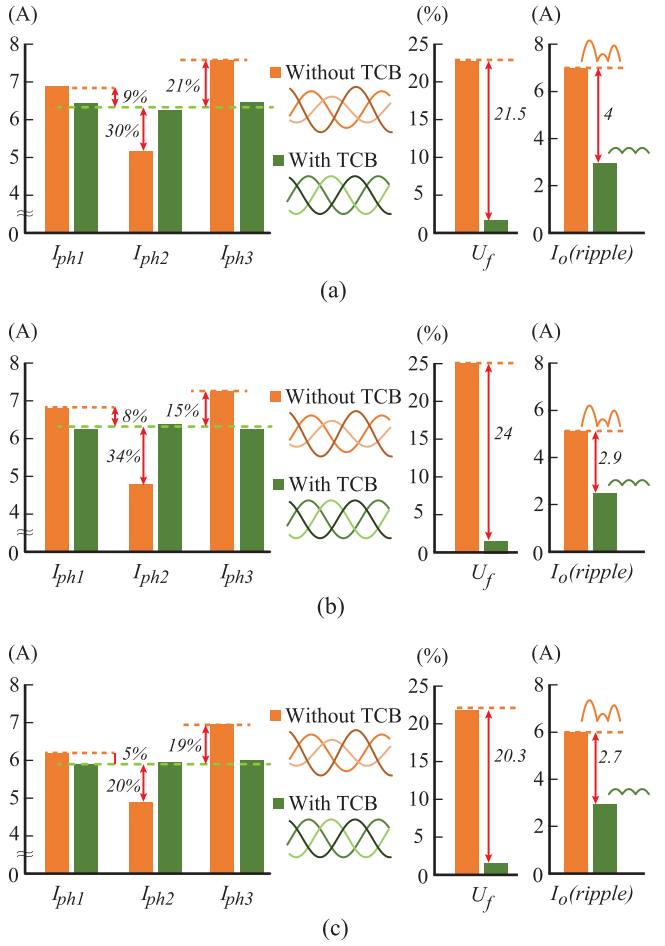

Fig. 14. Experimental results: primary currents RMS values and output current ripple values of the real circuit without TCB versus with TCB. (a) Below resonant frequency. (b) At resonant frequency. (c) Above resonant frequency. Using TCB, the primary currents are balanced, and the output current ripple is decreased by more than 50%.

As mentioned earlier, the converter has been tested under the worst-case unbalanced scenario. Fig. 11 shows the simulation results of the ideal balanced circuit versus the experimental results of the real unbalanced circuit. Fig. 11(a) shows the results at the resonant frequency, Fig. 11(b) shows the results above the resonant frequency, and Fig. 11(c) shows the results below the resonant frequency. As can be seen, the output current ripple of the unbalanced circuit is more than double the value in ideal balanced circuit. That is the main disadvantage of the unbalanced behavior in a three-phase LLC resonant converter. Uneven distribution of currents among the phases is the other disadvantage of the unbalanced behavior of the converter, which results in unequally distributed losses and unequally thermal distribution. Depending on the deviation in the normal values of the currents, this also results in slightly lower efficiency, which is caused by higher peak currents and higher conduction losses. The exact values of three-phase currents, as well as the efficiencies of each operation mode, are shown in Table IV.

As mentioned previously, the resonant components' values are corresponding to the scenarios II and IV discussed in Section II. In order to validate the current-sharing trend pre-

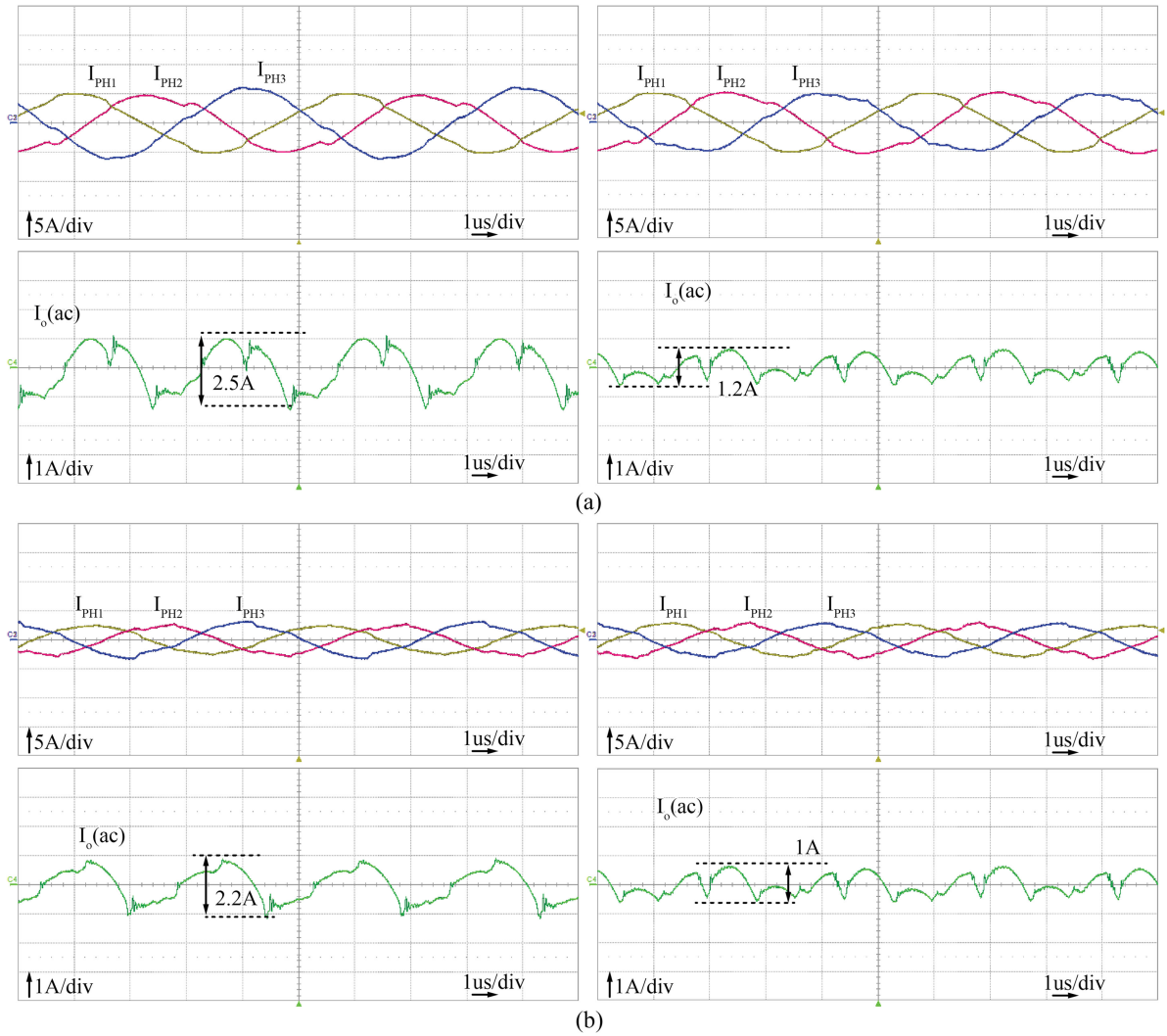

Fig. 15. Experimental results of the unbalanced circuit without TCB (left-hand side) versus the results of TCB (right-hand side) at resonant frequency. (a) At 50% of full-load. (b) At 10% of full-load. TCB decreases the output current ripple and improves the performance of the converter at different load conditions.

diction ability by the proposed analysis, the plots are presented in Fig. 12. In this figure, the analytical results of the normalized current values over the frequency range versus the experimental results are shown. As it can be seen, both the experimental and analytical results show the same trend of changes in the values of the currents with correspondence with the given resonant components' values in Table III. As the results show, phase 3 has the highest current, whereas phase 2 has the lowest current.

In order to verify the proposed TCB, this technique has been applied to the unbalanced circuit discussed above. Fig. 13 shows the results of the balancing technique versus the results of the unbalanced circuit with basic 120° modulation. This figure clearly shows that the TCB results in considerable reduction in the output current ripple and balances the RMS values of the currents through the phases. In Table IV, the experimental results of the current values, unbalanced factor (U_f), efficiency, output current ripple, and the phase angles of the input voltages in the ideal circuit, the unbalanced circuit, and TCB, are presented. The comparison of primary currents under different operating modes, unbalanced factor (U_f), and also current ripples for different conditions are presented in Fig. 14. This figure clearly confirms that the proposed method can successfully balance the currents in an unbalanced three-phase LLC resonant converter resulting in significant reduction in the output capacitor current ripple and even distribution of losses through the circuit. Table IV presents the final values of the voltage vector angles used by the TCB to balance the currents. According to the table, the largest deviation in the value of voltage vector angles happens above the resonant frequency, where TCB applies 34 phase shift on the phase 1 input voltage. Moreover, the efficiency is improved using TCB. For example, at resonant frequency, the efficiency of the real unbalanced circuit is improved by 0.4% points using TCB, which means around 12 W less losses at full load operation.

Moreover, in order to show the performance of the proposed TCB in different load levels, the test results of light-load and half-load conditions are provided in Fig. 15 and Table V. The results validate the performance of the proposed TCB for different power levels. It is clear that the worst case of unbalanced currents happens at full-load condition and the issue of the un-

TABLE V
EXPERIMENTAL RESULTS AT RESONANT FREQUENCY BEFORE AND AFTER TCB

Parameters	Before TCB		
	Full-load	Half-load	Light-load
Primary currents (rms) [A]	$I_{ph1}: 6.8$ $I_{ph2}: 4.7$ $I_{ph3}: 7.3$	$I_{ph1}: 3.8$ $I_{ph2}: 3.3$ $I_{ph3}: 4.5$	$I_{ph1}: 2.3$ $I_{ph2}: 2.7$ $I_{ph3}: 2.1$
Output current ripple [A]	5.3	2.5	2.2
Unbalanced factor (U_f)	25.6%	20.5%	17%
Parameters	After TCB		
	Full-load	Half-load	Light-load
Primary currents (rms) [A]	$I_{ph1}: 6.26$ $I_{ph2}: 6.3$ $I_{ph3}: 6.36$	$I_{ph1}: 3.8$ $I_{ph2}: 3.95$ $I_{ph3}: 3.85$	$I_{ph1}: 2.35$ $I_{ph2}: 2.45$ $I_{ph3}: 2.35$
Output current ripple [A]	2.4	1.2	1
Unbalanced factor (U_f)	1.5%	2.5%	2.8%

The results verify the effectiveness of the proposed TCB at different load levels.

balanced currents is less critical in light-load conditions. The proposed TCB technique can perfectly balance the currents, reduce the output current ripple, and improve the performance of the converter at any load condition. In fact, the results show that the performance of the proposed TCB does not depend on the load.

V. CONCLUSION

In this paper, an analysis of the current-sharing behavior of three-phase LLC resonant converter in correspondence to the resonant components' tolerances has been presented and discussed. Moreover, a TCB technique to improve the unbalanced behavior of the converter has been presented. The proposed TCB manipulates the phase shift between the inverter legs to balance the currents through the phases. This will result in significant decrease in the output current ripple, which allows the use of smaller output capacitor filter. Moreover, this technique results in equally distributed losses in the circuit, which makes thermal management of the circuit easier. As a result of even current-sharing among phases, no component experiences higher temperature or larger current than the expected current peaks and so it is possible to select components with lower power rating. In order to show the validity of the presented analysis and also the functionality of TCB, a 3-kW experimental prototype for PHEV application has been developed and tested. The experimental results show the validity of the presented current-sharing analysis with a good approximation, and also the validity of the proposed TCB.

REFERENCES

[1] Y. Wang, S. Gao, Y. Guan, J. Huang, D. Xu, and W. Wang, "A single-stage LED driver based on double LLC resonant tanks for automobile headlight with digital control," *IEEE Trans. Transp. Electrific.*, vol. 2, no. 3, pp. 357–368, Sep. 2016.

[2] C. Liu, H. Liu, G. Cai, S. Cui, H. Liu, and H. Yao, "Novel hybrid LLC resonant and DAB linear DCDC converter: Average model and experimental verification," *IEEE Trans. Ind. Electron.*, vol. 64, no. 9, pp. 6970–6978, Mar. 2017.

[3] J. Liu, J. Zhang, T. Q. Zheng, and J. Yang, "A modified gain model and the corresponding design method for an LLC resonant converter," *IEEE Trans. Power Electron.*, vol. 32, no. 9, pp. 6716–6727, Oct. 2016.

[4] R. Beiranvand, M. R. Zolghadri, B. Rashidian, and S. M. H. Alavian, "Optimizing the LLCLC resonant converter topology for wide-output-voltage and wide-output-load applications," *IEEE Trans. Power Electron.*, vol. 26, no. 11, pp. 3192–3204, Nov. 2011.

[5] W. Sun, H. Wu, H. Hu, and Y. Xing, "Modified LLC resonant converter with secondary paralleled bidirectional switch for applications with hold-up time requirement," *IET Power Electron.*, vol. 10, no. 3, pp. 398–404, Mar. 2017.

[6] M. A. Saket, N. Shafiei, and M. Ordonez, "LLC converters with planar transformers: Issues and mitigation," *IEEE Trans. Power Electron.*, vol. 32, no. 6, pp. 4524–4542, Jun. 2017.

[7] H. Valipour and M. Ordonez, "High efficiency LC resonant boost topology: Analysis and design," *IEEE Energy Convers. Congr. Expo.*, 2017, pp. 3427–3432.

[8] C. Hua, Y. Fang, and C. Lin, "LLC resonant converter for electric vehicle battery chargers," *IET Power Electron.*, vol. 9, no. 12, pp. 2369–2376, Oct. 2016.

[9] H. N. Vu and W. J. Choi, "A novel dual full-bridge LLC resonant converter for CC and CV charges of batteries for electric vehicles," *IEEE Trans. Ind. Electron.*, vol. 65, no. 3, pp. 2212–2225, Mar. 2018.

[10] H. Groot, E. Janssen, R. Pagano, and K. Schetters, "Design of a 1-MHz LLC resonant converter based on a DSP-driven SOI half-bridge power MOS module," *IEEE Trans. Power Electron.*, vol. 22, no. 6, pp. 2307–2320, Nov. 2007.

[11] S. V. G. Oliveira and I. Barbi, "A three-phase step-up DCDC converter with a three-phase high-frequency transformer for DC renewable power source applications," *IEEE Trans. Ind. Electron.*, vol. 58, no. 8, pp. 3567–3580, Oct. 2010.

[12] S. Bal, A. K. Rathore, and D. Srinivasan, "Naturally clamped snubberless soft-switching bidirectional current-fed three-phase pushpull DC/DC converter for DC microgrid application," *IEEE Trans. Ind. App.*, vol. 52, no. 2, pp. 1577–1587, Oct. 2015.

[13] H. Cha, J. Choi, and P. N. Enjeti, "A three-phase current-fed DC/DC converter with active clamp for low-DC renewable energy sources," *IEEE Trans. Power Electron.*, vol. 23, no. 6, pp. 2784–2793, Dec. 2008.

[14] L. P. Wong, D. K.-W. Cheng, M. H. L. Chow, and Y. S. Lee, "Interleaved three-phase forward converter using integrated transformer," *IEEE Trans. Ind. Electron.*, vol. 52, no. 5, pp. 1246–1260, Sep. 2005.

[15] D. S. Oliveira Jr, F. L. M. Antunes, and C. E. A. Silva, "A three-phase ZVS PWM DCDC converter associated with a double-wye connected rectifier, delta primary," *IEEE Trans. Power Electron.*, vol. 21, no. 6, pp. 1684–1690, Nov. 2006.

[16] J. Choi, H. Cha, and B.-M. Han, "A three-phase interleaved DCDC converter with active clamp for fuel cells," *IEEE Trans. Power Electron.*, vol. 25, no. 8, pp. 2115–2123, Aug. 2010.

[17] A. K. S. Bhat and R. L. Zheng, "A three-phase series-parallel resonant converter-analysis, design, simulation, and experimental results," *IEEE Trans. Ind. Appl.*, vol. 34, no., pp. 951–960, Jul./Aug. 1996.

[18] R. L. Zheng and A. K. S. Bhat, "Analysis and design of a three-phase LCC-type resonant converter," *IEEE Trans. Aerosp. Electron. Syst.*, vol. 34, no. 3, pp. 508–519, Jul. 1998.

[19] S. Akre, M. G. Egan, and M. J. Willers, "Analysis and design of a new three-phase LCC-type resonant DC-DC converter with capacitor output filter," *IEEE 31st Annu. Power Electron. Spec. Conf.*, 2000, pp. 721–728.

[20] M. S. Almardy and A. K. S. Bhat, "Three-phase (LC)(L)-type series-resonant converter with capacitive output filter," *IEEE Trans. Power Electron.*, vol. 26, no. 4, pp. 1172–1183, Apr. 2011.

[21] M. Kobayashi and M. Yamamoto, "Current balance performance evaluations for transformer-linked three phase DC-DC LLC resonant converter," *Int. Conf. Renew. Energy Res. Appl.*, pp. 1–3, 2012.

[22] S. A. Arshadi, M. Ordonez, M. Mohammadi, and W. Eberle, "Efficiency improvement of three-phase LLC resonant converter using phase shedding," *IEEE Energy Convers. Congr. Expo.*, pp. 3771–3775, 2017.

[23] E. Asa, K. Colak, M. Bojarski, and D. Czarkowski, "Three phase LLC resonant converter with D-DLL control technique for EV battery chargers," *IEEE Int. Electric Veh. Conf.*, pp. 1–7, 2014.

[24] M. Noah *et al.*, "A novel three-phase LLC resonant converter with integrated magnetics for lower turn-off losses and higher power density," *IEEE Appl. Power Electron. Conf. Expo.*, 2017, pp. 322–329.

[25] W. Martinez *et al.*, "Three-phase LLC resonant converter with integrated magnetics," *IEEE Energy Convers. Congr. Expo.*, pp. 1–8, 2016.

[26] Y. Nakakohara, H. Otake, T. M. Evans, T. Yoshida, M. Tsuruya, and K. Nakahara, "Three-phase LLC series resonant DC/DC converter using SiC MOSFETs to realize high-voltage and high-frequency operation," *IEEE Trans. Ind. Electron.*, vol. 63, no. 4, pp. 2103–2110, Apr. 2016.
[27] E. Orietti, P. Mattavelli, G. Spiazzi, C. Adragna, and G. Gattavari, "Current sharing in three-phase LLC interleaved resonant converter," *IEEE Energy Convers. Congr. Expo.*, 2009, pp. 1145–1152.
[28] H. S. Kim, J. W. Baek, and J. H. Jung, "Output current balancing method for three-phase interleaved LLC resonant converter employing Y-connected rectifier," *IEEE Appl. Power Electron. Conf. Expo.*, 2014, pp. 1227–1232.
[29] H. S. Kim, J. W. Baek, M. H. Ryu, J. H. Kim, and J. H. Jung, "The high-efficiency isolated AC-DC converter using the three-phase interleaved LLC resonant converter employing the y-connected rectifier," *IEEE Trans. Power Electron.*, vol. 29, no. 8, pp. 4017–4028, Aug. 2014.
[30] Z. Hu, Y. Qiu, L. Wang, and Y. F. Liu, "An interleaved LLC resonant converter operating at constant switching frequency," *IEEE Trans. Power Electron.*, vol. 29, no. 6, pp. 2931–2943, Jun. 2014.
[31] K. Murata and F. Kurokawa, "An interleaved PFM LLC resonant converter with phase-shift compensation," *IEEE Trans. Power Electron.*, vol. 31, no. 3, pp. 2264–2272, Mar. 2016.
[32] D. Moon, J. Park, and S. Choi, "New interleaved current-fed resonant converter with significantly reduced high current side output filter for EV and HEV applications," *IEEE Trans. Power Electron.*, vol. 30, no. 8, pp. 4264–4271, Aug. 2015.

Sayed Abbas Arshadi (S'16) was born in Isfahan, Iran. He received the B.Sc. degree in electrical engineering from the Malik Ashtar University of Technology, Isfahan, Iran, in 2012, and the M.Sc. degree in electrical engineering (Electronics) from the Isfahan University of Technology (IUT), Isfahan, Iran, in 2015. He is currently working toward the Ph.D. degree at the University of British Columbia (UBC), Vancouver, BC, Canada where he is the holder of a four-year fellowship.

From 2013 to 2016, he was a Researcher with the Information and Communication Technology Institute, Isfahan, Iran, where he was involved in the design and implementation of power converters. He has been also a Research Scholar with Delta-Q Technologies, Burnaby, BC, Canada, since 2016. His current research interests include medium- and high-power dc–dc resonant converters for battery chargers and renewable energy applications.

Martin Ordonez (S'02–M'09) was born in Neuquen, Argentina. He received the Ing. degree in electronics engineering from the National Technological University, Cordoba, Argentina, in 2003, and the M.Eng. and Ph.D. degrees in electrical engineering from the Memorial University of Newfoundland (MUN), St. John's, NL, Canada, in 2006 and 2009, respectively.

He is currently the Canada Research Chair in Power Converters for Renewable Energy Systems and an Associate Professor with the Department of Electrical and Computer Engineering, University of British Columbia, Vancouver, BC, Canada. He is also the holder of the Fred Kaiser Professorship on Power Conversion and Sustainability at UBC. He was an Adjunct Professor with Simon Fraser University, Burnaby, BC, Canada, and MUN. His industrial experience in power conversion includes research and development at Xantrex Technology, Inc., Elgar Electronics, Corporation (now AMETEK Programmable Power in San Diego, California), Deep-Ing Electronica de Potencia, Rosario, Argentina, and TRV Dispositivos, Cordoba, Argentina. With the support of industrial funds and the Natural Sciences and Engineering Research Council, he has contributed to more than 140 publications and R&D reports.

Dr. Ordonez is a Guest Editor for the IEEE JOURNAL OF EMERGING AND SELECTED TOPICS IN POWER ELECTRONICS, an Associate Editor for the IEEE TRANSACTIONS ON POWER ELECTRONICS, and an Editor for the IEEE TRANSACTIONS ON SUSTAINABLE ENERGY. He serves on several IEEE committees, and reviews widely for IEEE/IET journals and international conferences. He was a recipient of the David Dunsiger Award for Excellence in the Faculty of Engineering and Applied Science (2009) and the Chancellors Graduate Award/Birks Graduate Medal (2006), and became a Fellow of the School of Graduate Studies, MUN.

Wilson Eberle (S'98–M'07) received the B.Sc., M.Sc., and Ph.D. degrees from the Department of Electrical and Computer Engineering, Queens University, Kingston, ON, Canada, in 2000, 2003, and 2008, respectively.

He is currently a tenured Associate Professor with the School of Engineering, University of British Columbia (UBC), Kelowna, BC, Canada. At UBC, he is the Founder and Leader of the Energy Systems and Power Electronics Laboratory. His industrial experience includes positions at Ford Motor Company, Windsor, ON, Canada, and at Astec Advanced Power Systems, Nepean, ON, Canada. His research interests include high-efficiency power conversion circuits and control techniques for a wide range of industrial and consumer applications. He is the author or coauthor of more than 70 technical papers published in various IEEE international conferences and IEEE journals.

Dr. Eberle has received research grants from the Natural Sciences and Engineering Research Council in Canada, the Canadian Foundation for Innovation, the University of British Columbia, the Kaiser Foundation for Higher Education, and various industry partners.

Mohammad Ali Saket (S'15) was born in Tehran, Iran. He received the B.Sc. degree in electrical engineering from the Amirkabir University of Technology, Tehran, Iran, in 2009, and the M.Sc. degree in power electronics from the Sharif University of Technology, Tehran, Iran, in 2011. He is currently working toward the Ph.D. degree at the University of British Columbia, Vancouver, BC, Canada.

His research interests include planar magnetics, conducted electromagnetic interference, dc–dc converters, and wireless power transfer. He is currently working toward high-efficiency and low-noise integrated magnetic structures for dc–dc converters.

Marian Craciun (M'00) received the B.Sc. degree in electronics engineering from the Polytechnic Institute of Bucharest, Bucharest, Romania, in 1989.

He has more than 20 years of experience in developing telecom and industrial power electronics products and sustaining engineering. His industrial experience includes positions at Energo repairs RENEL and Asea Brown Boveri Ltd., Bucharest; Argus Technologies, Ltd., and Alpha Technologies, Ltd., Burnaby, BC, Canada. He is currently a Power Electronics R&D Engineer with Delta-Q Technologies, Corporation, Vancouver, BC, Canada. His current research interests include high-power high-efficiency converter topologies, high-power-factor rectifiers, resonant converters, electric vehicles, and sustainable and renewable energy sources.

Chris Botting (M'04) received the B.Sc. degree in electrical engineering from Calvin College, Grand Rapids, MI, USA, in 2001.

He is currently the Manager of the Research Engineering, Delta-Q Technologies, Burnaby, BC, Canada, with responsibility for research activities, funding, university collaboration, technology roadmap, intellectual property, and battery test laboratory functions. From 2001 to 2012, he was a Lead Systems Engineer with Azure Dynamics, Burnaby, BC, Canada, a manufacturer of electric and hybrid electric commercial vehicles, with responsibility for energy storage, high-voltage distribution and auxiliary systems, and powertrain architecture. His research interests include high-efficiency power converters, electric drive, energy storage, and renewable energy.